HIGH ORDER CONSERVATIVE SCHEMES FOR THE GENERALIZED BENJAMIN-ONO EQUATION IN THE UNBOUNDED DOMAIN

KAI YANG

ABSTRACT. This paper proposes a new class of mass or energy conservative numerical schemes for the generalized Benjamin-Ono (BO) equation on the whole real line with arbitrarily high-order accuracy in time. The spatial discretization is achieved by the pseudo-spectral method with the rational basis functions, which can be implemented by the Fast Fourier transform (FFT) with the computational cost $\mathcal{O}(N \log(N))$. By reformulating the spatial discretized system into the different equivalent forms, either the spatial semi-discretized mass or energy can be preserved exactly under the continuous time flow. Combined with the symplectic Runge-Kutta, with or without the scalar auxiliary variable reformulation, the fully discrete energy or mass conservative scheme can be constructed with arbitrarily high-order temporal accuracy, respectively. Our numerical results show the conservation of the proposed schemes, and also the superior accuracy and stability to the non-conservative (Leap-frog) scheme.

1. INTRODUCTION

This paper considers the numerical methods for solving the generalized Benjamin-Ono (gBO) equation

$$(1.1) \qquad \begin{cases} u_t = -(-\mathcal{H}u_x + \frac{1}{m}u^m)_x, & x \in \mathbb{R}, \ t > 0, \ m \in \mathbb{Z}^+, \\ u(x,0) = u_0, \end{cases}$$

where the Hilbert transform $\mathcal{H}$ is defined by

$$(1.2) \qquad \mathcal{H}f(x) = \frac{1}{\pi}\text{p.v.}\int_{-\infty}^{\infty}\frac{f(y)}{x-y}dy,$$

or equivalently, $\widehat{\mathcal{H}f}(\xi) = -i\,\text{sgn}(\xi)\hat{f}(\xi)$ on the Fourier frequency side. When $m = 2$, it is the well-known Benjamin-Ono (BO) equation

$$(1.3) \qquad u_t - \mathcal{H}u_{xx} + u_x u = 0,$$

derived by Benjamin [5] in 1967 and Ono [52] in 1975. This equation (1.3) models the one-dimensional waves in deep water. The BO equation is closely related to the Korteweg-de Vries (KdV) equation, where the Hilbert transform term $\mathcal{H}u_{xx}$ is replaced by u_{xxx}. The KdV

1

equation models the one-dimensional shallow water waves. Both equations, BO and KdV, are completely integrable. For example, the Lax pair can be constructed as described in e.g., [50], [33] [3], [26] and [2]. Other nonlinearities for the equation (1.1) are also considered. They are relevant in various other models of water waves, e.g., see [21], [1], [7] and [8]. When $m = 3$, the equation (1.1) is typically referred to as the modified Benjamin-Ono (mBO) equation. When $m \geq 3$, the equation (1.1) is typically referred to as the generalized Benjamin-Ono (gBO) equation. In general, the gBO equation (1.1) conserves the following three quantities

$$(1.4) \qquad I[u(t)] \stackrel{\text{def}}{=} \int u(x,t)dx = I[u_0];$$

$$(1.5) \qquad M[u(t)] \stackrel{\text{def}}{=} \int [u(x,t)]^2 dx = M[u_0];$$

$$(1.6) \qquad E[u(t)] \stackrel{\text{def}}{=} \int \left[\frac{1}{2} \left((\mathcal{H}\partial_x)^{\frac{1}{2}} u(x,t) \right)^2 - \frac{1}{m(m+1)} (u(x,t))^{m+1} \right] dx = E[u_0].$$

The first one is called the L^1-type integral, and the last two are often called mass and energy (Hamiltonian), respectively.

Besides its physical applications, the gBO equation is also interesting to study from the mathematical point of view. The well-posedness theory for the Cauchy problem has been discussed initially in [59] and [36]. Futher improvements on the well-posedness questions were done in [39], [34], [63], [16], [49], [48], [15], [66]. We also mention that when $m \geq 3$, it is typically referred to as the L^2-critical and L^2-supercritical cases from the scaling invariance, respectively. In those cases, there may exist blow-up solutions. This was numerically observed in [9] and our recent paper [55]. Besides the blow-up solutions, there are still many open questions, such as the soliton stability and the dispersion limit. These kind of questions have been studied both numerically and analytically. Compared with the (generalized) KdV equation (e.g., [10], [29], [30], etc.), the gBO equation is less well studied (e.g., [47], [54] and review [58]). Therefore, a stable, efficient and accurate numerical algorithm would facilitate the future study.

Numerical investigations on the BO equation have been started some time ago. Related articles can be found in [9], [23], [64] for the domain truncation approach; [11], [12], [67] for the computation of the Hilbert transform on $\mathbb{R}$; [31], [14] for the pseudo-spectral method with the rational basis functions; and [13] for a comparison between the domain truncation and the pseudo-spectral method on $\mathbb{R}$. Despite some years of investigations, there are still far less studies about numerical methods for the gBO equations than the gKdV equations. To our best knowledge, there are no results concerning the conservative schemes for the gBO equation on the whole real line $\mathbb{R}$ so far. On the other hand, the conservative schemes are always preferable in simulating the PDE's with conserved quantities, especially for studying the long time solution behavior, since it generally possess good accuracy and stability. One possible reason is the numerical approximation of the Hilbert transform on $\mathbb{R}$, which is

not as well studied as on a finite domain. However, if considering the conventional domain truncation spatial discretization strategy (e.g., the finite difference or Fourier spectral methods), the Hilbert transform usually leads to a slow decaying function, and consequently, to a relatively large domain truncation error.

The purpose of this paper is to construct the conservative schemes for the gBO equation (1.1) on the whole real line $\mathbb{R}$, with arbitrarily high order accuracy in time. The spatial discretization is achieved by the rational basis functions with the pseudo-spectral approach from [31]. We prove that by reformulating into the different forms, and applying the Hermitian or anti-Hermitian properties of the resulting spatial semi-discretized system, either the spatial semi-discretized mass or energy will be preserved. For the temporal discretization, the Crank-Nicholson method with the conventional reformulation of the nonlinear potential term (e.g., see [24] for the nonlinear Schrödinger (NLS) equation case) will lead to the conservation of the mass and energy in the discrete time flow. Furthermore, the high order conservative scheme can be constructed from the scalar auxiliary variable (SAV) approach (see [61], [62] and [20], [68] for applications to dispersive PDEs). By using the symplectic Runge-Kutta (SRK) method, the three invariant quantities (1.4)-(1.6) (with proper modifications for energy (1.6)) will be preserved exactly in the discrete time flow. However, due to the limitation of the spatial discretization, we can only conserve either the discrete mass or the discrete energy in the space-time fully discrete sense. In fact, this strategy is universal. By a similar space-time discretization, it is easy to construct the conservative schemes for the gKdV equations and the structure-preserving schemes (the discrete mass and energy are preserved exactly at the same time) for the NLS equations, as well as their high dimensional generalization by applying the tensor product. This will be useful in studying the long time behavior of the solutions for those equations, as well as the slow decaying solutions, since the traditional domain truncation strategy (e.g., [43], [69], [44], and [28]) requires large computational domain, and consequently, it results in large number of nodes in spatial discretization.

This paper is organized as follows. In Section 2, we introduce the pseudo-spectral spatial discretization strategy from the rational basis functions. Then, we define the discrete inner product with respect to the collocation points from such rational basis functions. Finally, we give the mass-conservative or the energy-conservative spatial semi-discretized form of the gBO equation (1.1). In Section 3, we first introduce the Crank-Nicholson types of temporal discretization. We show that the Crank-Nicholson method with its conventional modification on the nonlinear term, will preserve the mass and energy exactly in the discrete time flow. Combining with the previous results in Section 2, we give two fully discretized schemes for the gBO equation, which conserve either the discrete mass or the discrete energy. Next, we consider the high-order conservative schemes achieved by the symplectic Runge-Kutta method with the SAV reformulation. From the classical argument (e.g. [19], [56] and [68]), we show that the reformulated system preserves the quantities (1.4)-(1.6) exactly in the discrete time flow. Again, combined with the spatial discretization results in Section 2, we

give two fully discretized schemes with high order temporal accuracy—one conserves the discrete mass and the other conserves the discrete energy. In Section 4, we illustrate the numerical examples. As a comparison, we also show the numerical results obtained from the non-conservative semi-implicit Leap-Frog scheme. Our numerical results show that the proposed schemes preserve the designate quantities based on the type of conservative scheme we choose. Compared with the non-conservative scheme, these conservative schemes also possess better accuracy. Additionally, the error from the temporal discretization decreases on the order as expected (second order for the IRK2 and Leap-Frog schemes, and fourth order for the IRK4 schemes). These results show the validity and efficiency of the numerical methods proposed.

2. Spatial discretization

In this section, we describe the rational basis functions in $\mathbb{R}$ used for the spatial discretization. The review of basis functions can be found in [18] and [67]. One advantage of this discretization is that it can easily represent the Hilbert transform. Then, we define the discrete inner product corresponding to the collocation points from the rational basis functions. Finally, we introduce two types of the spatial discretization for the gBO equation (1.1): one is mass-conservative and the other one is energy-conservative.

2.1. **Rational basis functions.** Consider the rational basis functions on the whole real line $\mathbb{R}$,

$$(2.1) \qquad u(x,t) = \sum_{k=-\infty}^{\infty} \hat{u}_k(t)\rho_k(x), \quad \rho_k(x) = \frac{(\alpha+ix)^k}{(\alpha-ix)^{k+1}},$$

where α is a mapping parameter that we will describe later. In [18], it is shown that $\{\rho_k(x)\}_{k=-\infty}^{\infty}$ form a complete orthogonal basis in $L^2(-\infty,\infty)$ with the following orthogonality

$$(2.2) \qquad \int_{-\infty}^{\infty} \rho_j(x)\overline{\rho_k(x)}dx = \begin{cases} \pi/\alpha, & j=k \\ 0, & j\neq k. \end{cases} \overset{\text{def}}{=} \frac{\pi}{\alpha}\delta_{j,k}.$$

Therefore, we have

$$\hat{u}_k(t) = \frac{\alpha}{\pi}\int_{-\infty}^{\infty} u(x,t)\rho_k(x)dx.$$

From the rational expansion (2.1), the Hilbert transform can be easily calculated [67] by

$$(2.3) \qquad \mathcal{H}(u(t,x)) = \sum_{k=-\infty}^{\infty} -i\hat{u}_k(t)\text{sgn}(k)\rho_k(x),$$

with $\mathrm{sgn}(k) = 1$ when $k = 0$. Meanwhile, the derivatives of $u(x,t)$ can be computed by the relation

$$(2.4) \qquad u_x(x,t) = \sum_{k=-\infty}^{\infty} \frac{i}{2\alpha}[k\hat{u}_{k-1} + (2k+1)\hat{u}_k + (k+1)\hat{u}_{k+1}]\rho_k(x),$$

and higher order derivatives could be done iteratively.

In numerical computations, a truncation of N-term interpolation function $I_N u$ are used to approximate the function $u(x)$, i.e.,

$$u(x,t) \approx I_N u \overset{\text{def}}{=} \hat{\mathbf{u}}^T \vec{\rho} := \sum_{k=-N/2}^{N/2-1} \hat{u}_k(t)\rho_k(x),$$

where $\hat{\mathbf{u}} = (\hat{u}_{-N/2}, \hat{u}_{-N/2+1}, \cdots, \hat{u}_{N/2-1})^T$ is the vector of the truncated coefficients, and $\vec{\rho} = (\rho_{-N/2}(x), \cdots, \rho_{N/2-1}(x))^T$ is the vector function of $\rho_k(x)$. This leads to the sparse matrix forms

$$(2.5) \qquad u_x \approx [\mathbf{S_1}\hat{\mathbf{u}}]^T \vec{\rho}, \quad u_{xx} \approx [\mathbf{S_2}\hat{\mathbf{u}}]^T \vec{\rho}, \quad \mathcal{H}u \approx [\mathbf{H}\hat{\mathbf{u}}]^T \vec{\rho},$$

where $\mathbf{S_1}$ is given in (2.4) via the coefficients of $\{\hat{u}_k\}$, and $\mathbf{S_2} = \mathbf{S_1} \times \mathbf{S_1}$ by computing the derivatives iteratively from (2.4), and $\mathbf{H} = -i\mathrm{diag}(\mathrm{sgn}(-N/2+0.5), \cdots, \mathrm{sgn}(N/2-0.5))$ is the diagonal matrix representing the approximation of the Hilbert transform in (2.3).

From (2.4) and (2.5), it is easy to see that the matrices $\mathbf{S_1}$ and $\mathbf{H}$ are anti-Hermitian, and the matrix $\mathbf{S_2}$ is real and symmetric.

Now, consider the change of variable

$$x = \alpha \tan\frac{\theta}{2}, \quad \text{or equivalently,} \quad e^{i\theta} = \frac{\alpha + ix}{\alpha - ix}, \quad -\pi \le \theta \le \pi,$$

and a spatial discretization $x_j = \alpha \tan\frac{\theta_j}{2}, \theta_j = jh, h = 2\pi/N, j = -N/2, \cdots, N/2-1$, where the α is the mapping parameter indicating that $N/2$ collocation points are located in the interval $[-\alpha, \alpha]$. Notice that

$$(2.6) \qquad u(x_j) = \sum_{k=-N/2}^{N/2-1} \hat{u}_k \rho_k(x_j) \;\Rightarrow\; u(x_j)(\alpha - ix_j) = \sum_{k=-N/2}^{N/2-1} \hat{u}_k e^{ik\theta_j},$$

hence, the Fast Fourier transform (FFT) can be applied to obtain the coefficients $\hat{u}_k$. We note that the above discretization in space is not uniform in x, but uniform in θ, and the singularity at $x_{-N/2} = -\infty$ can be removed by imposing the boundary condition $u(-\infty) = 0$, i.e., $u_{-N/2} = 0$.

We denote the matrix $\mathbf{F}$ to be the standard Fast Fourier transform (FFT) matrix with $\{k\theta_j\}$, i.e.,

$$\mathbf{F}_{kj} = \frac{1}{N}e^{-ik\theta_j}, \quad \mathbf{F}^{-1}_{jk} = e^{ik\theta_j}, \quad -N/2 < j, k < N/2-1.$$

Note that instead of writing explicitly, the matrices $\mathbf{F}$ and $\mathbf{F}^{-1}$ can be computed by FFT, (see, e.g., [60, Chapter 2] and [65, Chapter 3]). Denote the diagonal matrix $\mathbf{P} = \mathrm{diag}(\alpha -$

$ix_{-N/2}, \cdots, \alpha - ix_{N/2-1})$ to be the weight matrix, which comes from (2.6). The coefficients $\hat{u}_k$ in the vector form can be represented by

$$(2.7) \qquad \hat{\mathbf{u}} = \mathbf{FPu},$$

where $\mathbf{u} = (u_{-N/2}, \cdots, u_{N/2-1})^T$ and $u_j = u(x_j)$.

Now, we define the discrete inner product with respect to the rational basis function. Denote the inner product between the two functions $u(x)$ and $v(x)$ on $\mathbb{R}$ by

$$\langle u(x), v(x) \rangle \overset{\text{def}}{=} \int_{\mathbb{R}} u(x)\bar{v}(x)dx.$$

Recall that the interpolation function $I_N u$ is the approximation of $u(x) \approx I_N u = \sum_{k=-N/2}^{N/2-1} \hat{u}_k \rho_k(x)$, then, the approximation of the inner product for functions u and v will be

$$(2.8) \qquad \langle u, v \rangle \approx \int_{\mathbb{R}} I_N u \overline{I_N v}\, dx = \frac{\pi}{\alpha} \sum_{k=-N/2}^{N/2-1} \hat{u}_k \bar{\hat{v}}_k$$

$$= \frac{\pi}{\alpha}(\overline{\mathbf{FPv}})^{\mathbf{T}}(\mathbf{FPu}) = \frac{\pi}{\alpha}\bar{\mathbf{v}}^{\mathbf{T}}\bar{\mathbf{P}}\bar{\mathbf{F}}^{\mathbf{T}}\mathbf{FPu} = \frac{\pi}{\alpha N}\bar{\mathbf{v}}^{\mathbf{T}}\bar{\mathbf{P}}\mathbf{Pu},$$

from the orthogonal property (2.2), the relation (2.7), and $\bar{\mathbf{F}}^{\mathbf{T}} = \frac{1}{N}\mathbf{F^{-1}}$ (e.g., see [60, Chapter 2]). Denote the diagonal matrix $\mathbf{W} = \mathbf{P}\bar{\mathbf{P}} = \text{diag}(\alpha^2 + x_{-N/2}^2, \cdots, \alpha^2 + x_{N/2-1}^2)$ to be the product of the two diagonal matrices $\mathbf{P}$ and $\bar{\mathbf{P}}$. According to (2.8), we can define the discrete inner product with respect to the collocation points $\{x_j\}$ from the rational basis function as follows:

$$(2.9) \qquad \langle \mathbf{u}, \mathbf{v} \rangle_h \overset{\text{def}}{=} \frac{\pi}{N\alpha}\bar{\mathbf{v}}^{\mathbf{T}}\mathbf{Wu} = \frac{\pi}{N\alpha} \sum_{j=-N/2}^{N/2-1} w_j u_j \bar{v}_j,$$

where $w_j = \alpha^2 + x_j^2$ can be considered as the weights for the quadrature.

2.2. **Conservative spatial discretization.** To discuss the conservative spatial discretizations, we first define the spatial semi-discretized L^1-type integral, mass and energy from (1.4)-(1.6). Let $\mathbf{1} = (1, 1, \cdots, 1)^T$ be the $N \times 1$ vector. For simplicity, we also denote by $\mathbf{u^m} = (u_{-N/2}^m, \cdots u_{N/2-1}^m)^T$ to be the pointwise power of the vector $\mathbf{u}$. Then, the spatial semi-discretized L^1-type integral, mass and energy are defined as follows

$$(2.10) \qquad I_h = \langle \mathbf{u}, \mathbf{1} \rangle_h;$$

$$(2.11) \qquad M_h = \langle \mathbf{u}, \mathbf{u} \rangle_h;$$

$$(2.12) \qquad E_h = \frac{1}{2}\langle \mathbf{P^{-1}F^{-1}HS_1FPu}, \mathbf{u} \rangle_h - \frac{1}{m(m+1)}\langle \mathbf{u^m}, \mathbf{u} \rangle_h.$$

It is easy to see that if $\mathbf{u} \in \mathbb{R}^N$, then $\frac{d}{dt}I_h = \langle \mathbf{u}_t, \mathbf{1} \rangle_h$, and $\frac{d}{dt}M_h = 2\langle \mathbf{u}_t, \mathbf{u} \rangle_h$ from (2.9). We also note that

$$(2.13) \qquad \frac{d}{dt}E_h = \frac{1}{2}\left(\langle \mathbf{P^{-1}F^{-1}HS_1FPu}_t, \mathbf{u} \rangle_h + \langle \mathbf{P^{-1}F^{-1}HS_1FPu}, \mathbf{u}_t \rangle_h \right)$$

$$- \frac{1}{m(m+1)}\left(\langle (\mathbf{u^m})_t, \mathbf{u} \rangle_h + \langle \mathbf{u^m}, \mathbf{u}_t \rangle_h \right)$$

$$= \mathrm{Re}\left(\langle \mathbf{P^{-1}F^{-1}HS_1FPu}, \mathbf{u}_t \rangle_h \right) - \frac{1}{m}\langle \mathbf{u^m}, \mathbf{u}_t \rangle_h,$$

since $\langle \mathbf{P^{-1}F^{-1}HS_1FPu}, \mathbf{u}_t \rangle_h = \overline{\langle \mathbf{P^{-1}F^{-1}HS_1FPu}_t, \mathbf{u} \rangle_h}$, and

$$\langle (\mathbf{u^m})_t, \mathbf{u} \rangle_h = m\langle \mathbf{u^{m-1}u}_t, \mathbf{u} \rangle_h = m\langle \mathbf{u^m}, \mathbf{u}_t \rangle_h$$

from (2.9).

Now, we have the following proposition for the spatial conservative discretizations.

Proposition 2.1. *The following spatial semi-discretized equation to the gBO equation (1.1)*

$$(2.14) \qquad \mathbf{u}_t = -\mathbf{P^{-1}F^{-1}S_1FP}(-\mathbf{P^{-1}F^{-1}HS_1PFu} + \frac{1}{m}\mathbf{u^m})$$

conserves the spatial semi-discretized energy, i.e.,

$$(2.15) \qquad \frac{d}{dt}E_h = 0.$$

On the other hand, the following spatial semi-discretized equation to the gBO equation (1.1)

$$(2.16) \qquad \mathbf{u}_t = \mathbf{P^{-1}F^{-1}HS_2FPu} - \frac{1}{m+1}\left(\mathrm{diag}(\mathbf{u^{m-1}})\mathbf{P^{-1}F^{-1}S_1FPu} + \mathbf{P^{-1}F^{-1}S_1FPu^m} \right)$$

conserves the spatial semi-discretized mass, i.e.,

$$(2.17) \qquad \frac{d}{dt}M_h = 0.$$

Proof. Putting the equation (2.14) in (2.13) yields

(2.18)

$$\frac{d}{dt}E_h = \mathrm{Re}\left(\langle \mathbf{P^{-1}F^{-1}HS_1FPu} - \frac{1}{m}\mathbf{u^m}, \mathbf{P^{-1}F^{-1}S_1FP}(\mathbf{P^{-1}F^{-1}HS_1FPu} - \frac{1}{m}\mathbf{u^m}) \rangle_h \right)$$

$$= \frac{\pi}{\alpha N}\mathrm{Re}\left[\overline{\left(\mathbf{P^{-1}F^{-1}S_1FP}(\mathbf{P^{-1}F^{-1}HS_1FPu} - \frac{1}{m}\mathbf{u^m})\right)}^{\mathbf{T}} \mathbf{W}\left(\mathbf{P^{-1}F^{-1}HS_1FPu} - \frac{1}{m}\mathbf{u^m}\right)\right]$$

$$= \frac{\pi}{\alpha N}\mathrm{Re}\left[\overline{\left(\mathbf{P^{-1}F^{-1}HS_1FPu} - \frac{1}{m}\mathbf{u^m}\right)}^{\mathbf{T}} (\mathbf{\bar{P}F^{-1}S_1FP})^{\mathbf{T}}\left(\mathbf{P^{-1}F^{-1}HS_1FPu} - \frac{1}{m}\mathbf{u^m}\right)\right] = 0,$$

since the matrix $\frac{1}{N}\mathbf{\bar{P}F^{-1}S_1FP}$ is anti-Hermitian.

Similarly, we first note that $\mathbf{W}\mathrm{diag}(\mathbf{u^{m-1}}) = \mathrm{diag}(\mathbf{u^{m-1}})\mathbf{W}$, since both of them are diagonal matrices. Then,

$$(2.19) \qquad \frac{d}{dt}M_h = 2\langle \mathbf{u_t}, \mathbf{u}\rangle = 2\langle \mathbf{P^{-1}F^{-1}HS_2FPu}, \mathbf{u}\rangle_h$$

$$-\frac{2}{m+1}\langle\left(\mathrm{diag}(\mathbf{u^{m-1}})\mathbf{P^{-1}F^{-1}S_1FPu} + \mathbf{P^{-1}F^{-1}S_1FPu^m}\right), \mathbf{u}\rangle_h$$

$$= 0 - \frac{2\pi}{(m+1)\alpha N}\left((\mathbf{u^m})^{\mathbf{T}}\bar{\mathbf{P}}\mathbf{F^{-1}S_1FPu} + \mathbf{u^T}\bar{\mathbf{P}}\mathbf{F^{-1}S_1FPu^m}\right) = 0,$$

from the similar decomposition to (2.18), and the fact that the matrices $\frac{1}{N}\bar{\mathbf{P}}\mathbf{F^{-1}HS_2FP}$ and $\frac{1}{N}\bar{\mathbf{P}}\mathbf{F^{-1}S_1FP}$ are also anti-Hermitian. $\qquad\qquad\square$

3. TEMPORAL AND FULL DISCRETIZATION

In this section, we first discuss the temporal discretization, and then, the space-time full discretization of the gBO equation (1.1). We start with the most commonly used Crank-Nicholson-type scheme. After that, we consider the high order conservative schemes. This is achieved by the symplectic Runge-Kutta method, such as the Gauss-Legendre Runge-Kutta method. When considering the energy conservation, the scalar auxillary variabel (SAV) approach from [61] and [20] will be incorporated. With this kind of approach, one can easily construct the conservative numerical scheme with arbitrarily high order accuracy in time.

3.1. **Crank-Nicholson-type scheme.** We first introduce the notations. Assume that our simulation is on the finite time interval $t \in [0, T]$. Define τ to be the time step and $t_n = n\tau$ to be the time at the nth time step. Denote $u^n \approx u(x, t_n)$ to be the semi-discretization in time. Denote $I^n = I[u^n]$, $M^n = M[u^n]$ and $E^n = E[u^n]$ to be the momentum, mass and energy from (1.4)-(1.6) at time $t = t_n$. For convenience, the half-time step is denoted as $u^{n+\frac{1}{2}} = \frac{1}{2}(u^n + u^{n+1})$ from the linear interpolation. We also denote the full discretization by $u^n_j \approx u(x_j, t_n)$, and the column vector $\mathbf{u}^n \approx u(\mathbf{x}, t_n)$. Now, we define the discrete L^1-type integral, mass and energy as follows:

$$(3.1) \qquad\qquad I^n_h = \langle \mathbf{u}^n, \mathbf{1}\rangle_h;$$

$$(3.2) \qquad\qquad M^n_h = \langle \mathbf{u}^n, \mathbf{u}^n\rangle_h;$$

$$(3.3) \qquad\qquad E^n_h = \frac{1}{2}\langle \mathbf{P^{-1}F^{-1}HS_1FPu}^n, \mathbf{u}^n\rangle_h - \frac{1}{m(m+1)}\langle (\mathbf{u}^n)^{\mathbf{m}}, \mathbf{u}^n\rangle_h.$$

We propose the following Crank-Nicholson-type *mass-conservative* scheme.

Theorem 3.1. *The scheme*

$$(3.4) \quad \frac{\mathbf{u}^{n+1} - \mathbf{u}^n}{\tau} = \mathbf{P^{-1}F^{-1}HS_2FPu}^{n+\frac{1}{2}}$$

$$-\frac{1}{m+1}\left(\mathrm{diag}\left((\mathbf{u}^{n+\frac{1}{2}})^{\mathbf{m-1}}\right)\mathbf{P^{-1}F^{-1}S_1FPu}^{n+\frac{1}{2}} + \mathbf{P^{-1}F^{-1}S_1FP}(\mathbf{u}^{n+\frac{1}{2}})^{\mathbf{m}}\right)$$

conserves the discrete mass (3.2) *exactly in time, i.e.,*

$$M_h^{n+1} = M_h^n.$$

Proof. The proof is straightforward. Equipping the equation (3.4) with the discrete inner product (2.9) with the vector $\mathbf{u}^{n+\frac{1}{2}}$, and using the identity (2.19) in Proposition 2.1 yields the result. □

For the Crank-Nicholson-type *energy-conservative* scheme, by modifying of the nonlinear term, we have the following theorem.

Theorem 3.2. *The scheme*

(3.5)
$$\frac{\mathbf{u}^{n+1} - \mathbf{u}^n}{\tau} = \mathbf{P^{-1}F^{-1}S_1FP}\left[\mathbf{P^{-1}F^{-1}HS_1FPu}^{n+\frac{1}{2}}\right.$$
$$\left. - \frac{1}{m(m+1)}\mathrm{diag}\left(\frac{(\mathbf{u}^{n+1})^{\mathbf{m+1}} - (\mathbf{u}^n)^{\mathbf{m+1}}}{(\mathbf{u}^{n+1})^{\mathbf{2}} - (\mathbf{u}^n)^{\mathbf{2}}}\right)\mathbf{u}^{n+\frac{1}{2}}\right]$$

conserves the discrete energy (3.3) *exactly in time, i.e.,*

$$E_h^{n+1} = E_h^n.$$

Proof. Following the same idea as in Theorem 3.1, we equip the equation (3.5) with the discrete inner product (2.9) with the vector

$$\mathbf{P^{-1}F^{-1}HS_1FPu}^{n+\frac{1}{2}} - \frac{1}{m(m+1)}\mathrm{diag}\left(\frac{(\mathbf{u}^{n+1})^{\mathbf{m+1}} - (\mathbf{u}^n)^{\mathbf{m+1}}}{(\mathbf{u}^{n+1})^{\mathbf{2}} - (\mathbf{u}^n)^{\mathbf{2}}}\right)\mathbf{u}^{n+\frac{1}{2}}.$$

Then, using the identity (2.18) in Proposition 2.1 yields the result. □

The construction for the conservative schemes in Theorem 3.1 and Theorem 3.2 are standard. If we only consider the semi-discretization in time, the scheme (3.4) is the midpoint rule, or the implict 2nd order Runge-Kutta method (IRK2), which is also known as the symplectic (quadratic preserving) Runge-Kutta method. We split the potential into the form

$$\frac{1}{m}(u^m)_x = \frac{1}{m+1}[u^{m-1}u_x + (u^m)_x]$$

for the purpose of creating the symmetry for the mass conservations in the spatial discretization, which we discussed in the previous section. For the energy conservation, we need to reformulate the potential part, which is widely used in literature, see e.g., [22], [46] and [41] for the NLS case. It is easy to see that if we only consider the temporal semi-discretization (assuming the spatial variable is continuous), then the scheme (3.5) will conserve both the mass and energy in the discrete time flow.

We next discuss the numerical schemes with higher order temporal accuracy. For simplicity and conciseness, we only consider the semi-discretization in time. The space-time full discretization results can be easily generalized together with the results from Section 2.

3.2. **High order conservative schemes.** The high order temporal conservative schemes can be achieved by the symplectic Runge-Kutta (SRK) method. We first briefly review the RK method before showing our results. Consider the problem

$$(3.6) \qquad u_t = f(u).$$

From the time $t = t_n$ to $t = t_{n+1}$, let b_i, $a_{ij}(i, j = 1, \cdots s)$ be real numbers, and $c_i = \sum_{j=1}^{s} a_{ij}$ be the collocation points. Denote the intermediate values U_i to be the solution satisfying (3.6) at the intermediate time $t^i = t_n + \tau c_i$. Then, the intermediate values U_i's are calculated by

$$(3.7) \qquad U_i = u^n + \tau \sum_{j=1}^{s} a_{ij} f_j,$$

where $f_i = f(U_i)$. The solution u^{n+1} is updated by

$$(3.8) \qquad u^{n+1} = u^n + \tau \sum_{j=i}^{s} b_i f_i.$$

We usually write the coefficients $\mathbf{A} = (a_{ij})$, $\mathbf{b} = (b_1, b_2, \cdots, b_s)$ and $\mathbf{c} = (c_1, c_2, \cdots, c_s)^T$ in the Butcher's Tableaus ([17]):

$$\begin{array}{c|c} \mathbf{c} & \mathbf{A} \\ \hline & \mathbf{b} \end{array}.$$

For example, we list two commonly used Runge-Kutta methods in the Butcher's Tableaus in Table 1. They are the s-stage Runge-Kutta methods with $s = 1, 2$, respectively. These methods are coming from the Gaussian-Legendre quadrature, known as the IRK2 and IRK4 methods, since the temporal accuracy is on the order of 2 and 4, respectively. We use these methods in our numerical simulations in the next section. There are many other types of Runge-Kutta methods as well, we refer the interested reader to [6], [19], [56], [27] and [57].

$$\begin{array}{c|c} \frac{1}{2} & \frac{1}{2} \\ \hline & 1 \end{array}$$

(A) IRK2

$$\begin{array}{c|cc} \frac{1}{2} - \frac{1}{6}\sqrt{3} & \frac{1}{4} & \frac{1}{4} - \frac{1}{6}\sqrt{3} \\ \frac{1}{2} + \frac{1}{6}\sqrt{3} & \frac{1}{4} + \frac{1}{6}\sqrt{3} & \frac{1}{4} \\ \hline & \frac{1}{2} & \frac{1}{2} \end{array}$$

(B) IRK4

TABLE 1. Butcher's Tableaus for the s-stage Gaussian-Legendre collocation Runge-Kutta methods with $s = 1, 2$.

We prove the following theorem for the mass-conservative scheme.

Theorem 3.3. *The s-stage symplectic (quadratic preserving) Runge-Kutta method, which satisfies*

$$(3.9) \qquad b_i a_{ij} + b_j a_{ji} = b_i b_j, \qquad for \quad i, j = 1, \cdots, s,$$

conserves the discrete mass exactly in time for the spatial discretized gBO equation (2.16), *i.e.,*

$$M_h^{n+1} = M_h^n.$$

Proof. The proof is standard. From the standard RK theory (e.g., [19], [56]), we can show that the temporal semi-discretized scheme conserves the mass exactly in the discrete time flow. Indeed, the RK theory shows that

$$M^{n+1} - M^n = 2\tau \sum_{i=1}^{s} b_i \langle U_i, f(U_i) \rangle + \tau^2 \sum_{i,j=1}^{s} (b_i a_{ij} + b_j a_{ji} - b_i b_j) \langle f(U_i), f(U_j) \rangle = 0,$$

since $\langle U_i, f(U_i) \rangle = 0$ by putting $f(U)$ in the form of (1.1).

When considering the space-time full discratization, we have

$$M_h^{n+1} - M_h^n = 2\tau \sum_{i=1}^{s} b_i \langle \mathbf{U}_i, f(\mathbf{U}_i) \rangle_h + \tau^2 \sum_{i,j=1}^{s} (b_i a_{ij} + b_j a_{ji} - b_i b_j) \langle f(\mathbf{U}_i), f(\mathbf{U}_j) \rangle_h = 0,$$

where the vector $\mathbf{U}_i$ is the discretized version of the intermediate value U_i for $i = 1, \cdots, s$, and $\langle \mathbf{U}_i, f(\mathbf{U}_i) \rangle_h = 0$ by using the relation (2.19).

$\square$

The symplectic Runge-Kutta method cannot preserve the discrete energy. In order to construct the energy-preserving scheme, we need to reformulate the potential term in the same idea as in (3.5). This is achieved by using the scalar auxillary approach from [61] and [20]. We reformulate the equation (1.1) into an equivalent system as follows:

$$(3.10) \qquad \begin{cases} u_t = -\left(-\mathcal{H}u_x + \dfrac{1}{m} \dfrac{u^m v}{\sqrt{\langle u^m, u \rangle + C_0}} \right)_x, \\ v_t = \dfrac{m+1}{2\sqrt{\langle u^m, u \rangle + C_0}} \langle u^m, u_t \rangle, \end{cases}$$

with the initial condition

$$u(x,0) = u_0, \qquad v_0 = \sqrt{\langle u_0^m, u_0 \rangle + C_0}.$$

Then, the energy to the system (1.1) is modified into the equivalent form

$$(3.11) \qquad E[u(t), v(t)] \overset{\text{def}}{=} \frac{1}{2} \langle \mathcal{H}u_x, u \rangle - \frac{1}{m(m+1)}(v^2 - C_0) \equiv E[u_0, v_0].$$

Here, we slightly nabuse the notation $E[u, v]$ to represent the modified energy for convenience, since it is equivalent to the energy $E[u]$ in (1.6) in the continuous sense. The C_0 is a constant to make sure that the term $\langle u^m, u \rangle + C_0$ is positive for all time $t \in [0, T]$. In the actual computation, the C_0 is adjustable during the time evolution, and thus, we only need to choose the constant C_0 such that the term $\langle u^m, u \rangle + C_0 > 0$ in the time interval $t \in [t_n, t_{n+1}]$. This is easily fulfilled, since we only consider the solution smooth in time. We will discuss the C_0 adjustment process at the end of this subsection.

Denote $v^n \approx v(t_n)$ to be the semi-discretization of v in time, and also $v_h \approx v(\mathbf{u})$ to be the semi-discretization of v in space. We write the space-time full discretization of v as $v_h^n \approx v(\mathbf{u}^n, t_n)$. The reformulated equation system (3.11) can be discretized by the rational basis functions into the following form

$$(3.12) \quad \begin{cases} \mathbf{u}_t = -\mathbf{P^{-1}F^{-1}S_1FP}\left(-\mathbf{P^{-1}F^{-1}HS_1FP u} + \dfrac{1}{m}\dfrac{\mathbf{u^m} v_h}{\sqrt{\langle \mathbf{u^m,u}\rangle_h + C_0}}\right) \overset{\text{def}}{=} f(\mathbf{u}, v_h), \\ (v_h)_t = \dfrac{m+1}{2\sqrt{\langle \mathbf{u^m,u}\rangle_h + C_0}}\langle \mathbf{u^m}, \mathbf{u}_t\rangle_h \overset{\text{def}}{=} g(\mathbf{u}, v_h), \end{cases}$$

with the initial conditions

$$\mathbf{u}^0 = u(\mathbf{x}, 0), \qquad v_h^0 = \sqrt{\langle (\mathbf{u}^0)^{\mathbf{m}}, \mathbf{u}^0\rangle_h + C_0}.$$

The fully discrete modified energy is defined as follows

$$(3.13) \qquad E_h^n = \frac{1}{2}\langle \mathbf{P^{-1}F^{-1}HS_1FP u}^n, \mathbf{u}^n\rangle_h - \frac{1}{m(m+1)}\left((v_h^n)^2 - C_0\right).$$

Next, we prove the following theorem for the high order energy-conservative schemes.

Theorem 3.4. *The s-stage symplectic Runge-Kutta method, which satisfies (3.9), conserves the L^1-type integral (1.4), mass (1.5) and modified energy (3.11) in the discrete time flow for the reformulated gBO equation system (3.10), i.e.,*

$$(3.14) \qquad I^{n+1} = I^n, \quad M^{n+1} = M^n, \quad and \quad E^{n+1} = E^n.$$

Furthermore, the symplectic Runge-Kutta method preserves the discrete energy (3.13) for the spatial semi-discretized system (3.12), i.e.,

$$(3.15) \qquad E_h^n = E_h^{n-1} = \cdots = E_h^0.$$

Proof. The proof for the conservation of the temporal semi-discretized L^1-type integral, mass and energy (3.14) is standard, e.g., see [19], [56], [45] and our earlier paper [68].

For the proof of the discrete energy conservation (3.15), substituting the inner product into the discrete sense, straightforward calculations yield

$$
E_h^{n+1} = \frac{1}{2}\langle \mathbf{P^{-1}F^{-1}HS_1FPu}^{n+1}, \mathbf{u}^{n+1}\rangle_h - \frac{1}{m(m+1)}\left((v_h^{n+1})^2 - C_0\right)
$$

$$
= \frac{1}{2}\langle \mathbf{P^{-1}F^{-1}HS_1FP}(\mathbf{u}^n + \tau\sum_{i=1}^{s}b_i f(\mathbf{U}_i, V_i)), \mathbf{u}^n + \tau\sum_{i=1}^{s}b_i f(\mathbf{U}_i, V_i)\rangle_h
$$

$$
- \frac{1}{m(m+1)}\left((v_h^n + \tau\sum_{i=1}^{s}b_i g(\mathbf{U}_i, V_i))^2 - C_0\right)
$$

$$
= E_h^n + \tau\sum_{i=1}^{s}b_i\left(\langle \mathbf{P^{-1}F^{-1}HS_1FP}f(\mathbf{U}_i, V_i), \mathbf{U}_i\rangle_h - \frac{2}{m(m+1)}V_i g(\mathbf{U}_i, V_i)\right)
$$

$$
+ \tau^2\sum_{i,j=1}^{s}(b_i a_{ij} + b_j a_{ji} - b_i b_j)\left(\langle f(\mathbf{U}_i, V_i), f(\mathbf{U}_j, V_j)\rangle_h + g(\mathbf{U}_i, V_i)g(\mathbf{U}_j, V_j)\right)
$$

$$
= E_h^n
$$

by using the relation (2.18), (3.12) and (3.9), where V_i is defined as the intermediate value of v_h^n for (3.12) similar to (3.7) and (3.8).

$\square$

Remark 3.1. Comparing with the proof in [68, Theorem 3.1], the symplectic Runge-Kutta method can preserve all the three quantities in the discrete time flow for the reformulated system (3.10). However, due to the limitation of the spatial discretization, only the discrete energy will be preserved in the fully discrete sense. The conservation of the discrete momentum for the gKdV equations in [68] is obtained by using the circulant and anti-symmetric property of the first order differential matrix from the Fourier pseudo-spectral discretization. We note that the rational basis functions here do not possess this property.

The adjustment process for the constant C_0 from [68] can be adapted here. Suppose at $t = t_n$, the term $\int(u^n)^{m+1}dx + C_0 < Tol$, where Tol is a given positive number (e.g., $Tol = 5$). Then, we choose another constant $\tilde{C}_0$ such that $\int(u^n)^{m+1}dx + \tilde{C}_0 > Tol$. For example, we can take $\tilde{C}_0 = 10 - \int(u^n)^{m+1}dx$, which leads to our new $\tilde{v}^n \approx \sqrt{10}$. Then, by using $E[u^n, v^n] = E[u^n, \tilde{v}^n]$ from (3.11), we have our new $\tilde{v}^n$

$$(3.16) \qquad\qquad \tilde{v}^n = \sqrt{(v^n)^2 + \tilde{C}_0 - C_0}.$$

Finally, we substitute the v^n and C_0 in (3.10) with $\tilde{v}^n$ and $\tilde{C}_0$, and then, continue with the time evolution for $t = t_{n+1}, t_{n+2}, \cdots$.

Remark 3.2. Note that $v^2 = \int u^{n+1}dx + C_0$ holds only at the collocation points $t = t_n + \tau c_i$ for each $i = 1, 2, \cdots, s$ in $t \in [t_n, t_{n+1}]$. However, the constant c_i may not necessarily be equal to 0 or 1, e.g., see Table 1. This means $v^2 = \int u^{n+1}dx + C_0$ does not hold at t_n in

the discrete time flow. Therefore, the new $\tilde{v}^n$ can only be evaluated by (3.16) to keep the discrete energy (3.11) invariant.

4. Numerical results

In this section, we list our numerical examples for the proposed schemes. Before discussing the examples, we mention that a type of a fixed point iteration solver from [20] and [68] can be easily adapted here for solving the resulting nonlinear system from the IRK methods. The total computational cost is on the order of $\mathcal{O}(N \log(N))$ from FFT.

We denote by the IRK2-MC and IRK4-MC the mass conservative schemes for solving (2.16) by using the 1st and 2nd stage RK methods with Gauss-Legendre collocation points from Table 1. We also denote by the IRK2-EC and IRK4-EC the energy conservative schemes for solving the reformulated system (3.12). As a comparison, we use the commonly used 2nd order non-conservative semi-implicit Leap-Frog scheme as follows

$$(4.1) \qquad \frac{\mathbf{u}^{n+1} - \mathbf{u}^{n-1}}{2\tau} = -\mathbf{P}^{-1}\mathbf{F}^{-1}\mathbf{S_1}\mathbf{FP}\left(\mathbf{P}^{-1}\mathbf{F}^{-1}\mathbf{H}\mathbf{S_1}\mathbf{FP}\left(\frac{\mathbf{u}^{n+1} + \mathbf{u}^{n-1}}{2}\right) + \frac{1}{m}(\mathbf{u}^n)^{\mathbf{m}}\right),$$

denoted as Leap-Frog. We track the following quantities at $t = t_n$ to check the accuracy:

$$(4.2) \qquad\qquad\qquad \mathcal{E}^n = \|u^n_{exact} - \mathbf{u}^n\|_\infty;$$

$$(4.3) \qquad\qquad\qquad \mathcal{E}^n_I = \max_{l<n} |I^l_h - I^0_h|;$$

$$(4.4) \qquad\qquad\qquad \mathcal{E}^n_M = \max_{l<n} |M^l_h - M^0_h|;$$

$$(4.5) \qquad\qquad\qquad \mathcal{E}^n_E = \max_{l<n} |E^l_h - E^0_h|.$$

When the SAV approach is not applied (IRK2-MC , IRK4-MC and Leap-Frog), the discrete energy E^n_h is computed from (3.3); and when the SAV approach is applied, the discrete energy E^n_h is computed from the modified version (3.13). We mention here that it is easy to see the equivalence between the Crank-Nicholson scheme (3.4) and the IRK2-MC scheme. The energy-conservative Crank-Nicholson scheme, which (3.5) considers reformulating the potential, also shares the same idea as in the IRK2-EC scheme. We omit the numerical result from the Crank-Nicholson methods for the purpose of conciseness, though compared with the IRK2-EC scheme, the energy-conservative Crank-Nicholson scheme usually requires less iterations in the fixed point iteration process, since the SAV approach introduces an additional scalar variable.

Now, we are ready to illustrate examples for our numerical simulations.

Example 1. Our first example considers the soliton solution for the BO ($m = 2$) equation, $u(x,t) = \frac{4c}{1+c^2(x-x_0-ct)^2}$. These type of solutions come from the smooth, positive, decaying at infinity solitary wave solution to the profile equation

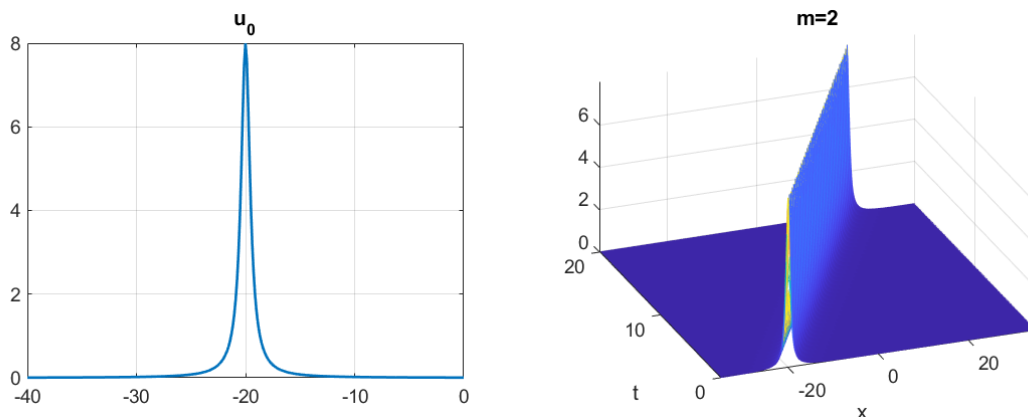$$(4.6) \qquad\qquad\qquad \mathcal{H}Q_x + cQ - \frac{1}{m}Q^m = 0,$$

FIGURE 1.   The solution profile for Example 1 from the IRK4-EC. Left: u_0.
Right: $u(x,t)$.

where c is a constant that indicates the speed of the traveling waves as well as the magniti-
tude. The solutions are expected to travel to the right as the solitons, for example from the
spectral stability result in [35], [4] and the inverse scattering theory [26], [32].

In our numerical simulations, we take $\alpha = 25$ with $N = 1024$. We take the traveling speed
$c = 2$ and starting point at $x_0 = -20$. The time step τ is taken to be $\tau = \frac{1}{20}$ for all the four
IRK type methods, and $\tau = \frac{1}{40}$ for the Leap-Frog scheme (4.1), since taking the $\tau = \frac{1}{20}$ will
lead to the numerical instability in our numerical computations for the Leap-Frog scheme.
We stop our numerical simulation at $T = 20$.

Figure 1 shows the solution profile obtained from the IRK4-EC scheme. The left subplot
is the initial condition u_0, the right subplot is the time evolution. One can see that the
solution travels in the solitary wave manner, which is previously observed in [31] and [55]
and also as expected.

Figure 2 tracks the results obtained from the different time integrators. The top left
subplot in Figure 2 shows $\|\mathbf{u}^n - u_{exact}\|_\infty$ with respect to time, where $u_{exact} = u(\mathbf{x}, t_n)$ is the
exact solution. One can see that the Leap-Frog scheme (4.1) has the largest error (see the
green circle line). Moreover, the 4th order schemes (IRK4-MC and IRK4-EC) own the better
accuracy than the second order schemes (IRK2-MC, IRK2-EC and Leap-Frog), which is as
expected, since they have higher order temporal accuracy. Furthermore, we observe that the
energy-conservative schemes (dash red line for IRK2-EC and dot purple line for IRK4-EC)
perform better than the mass-conservative schemes (blue solid line for IRK2-MC and orange
dash-dot line for IRK4-EC). Thus, the energy-conservative schemes are recommended for
future studies.

The top right subplot in Figure 2 tracks the error of the discrete L^1-type integral (4.3)
at different times. One can see that the more accurate the time integrators are, the better
preservation of this quantity will be, though they are not conserved exactly.
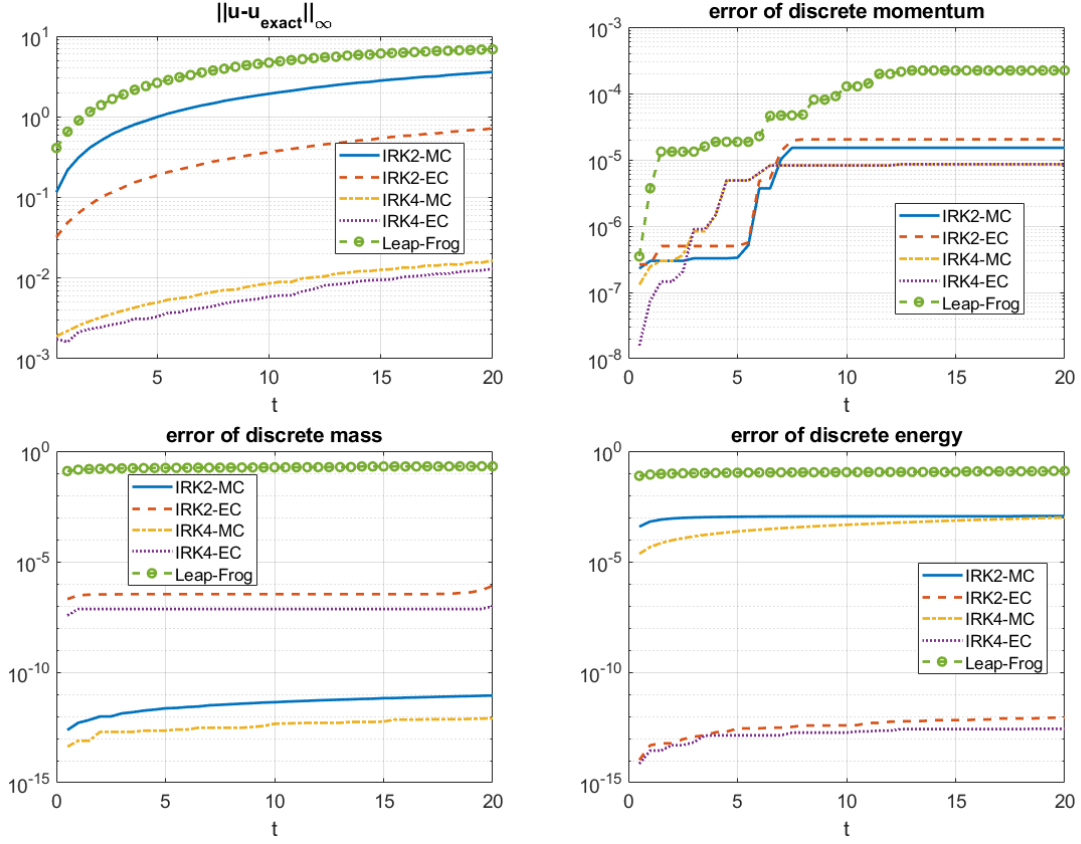
FIGURE 2. The errors in Example 1 by different time integrators: IRK2-MC (solid blue); IRK2-EC(dash red); IRK4-MC (dash dot orange); IRK4-EC (dot purple); Leap-Frog (circle green). Top left: $\|u - u_{exact}\|_\infty$. Top right: discrete momentum error. Bottom left: discrete mass error. Bottom right: discrete energy error.

The bottom two subplots in Figure 2 track the error of discrete mass (4.4) and energy (4.5), respectively. The mass-conservative schemes (IRK2-MC and IRK4-MC) keep the error of discrete mass below at the level of 10^{-12}, which is the tolerance of the fixed iteration in solving the resulting nonlinear system from the implicit Runge-Kutta method. On the other hand, the discrete mass error for the other types of schemes is relatively large, especially the Leap-Frog scheme (thus, refered to as least accurate).

The bottom right subplot tracks the error of the discrete energy. It shows that the energy-conservative schemes (IRK2-EC and IRK4-EC) keep the error of discrete mass below the level of 10^{-12}. This justifies the validity of our schemes. Similarly, for the other time integrators, the Leap-Frog scheme performs the worst even with a smaller time step τ,; the other two mass-conservative schemes keep the error of discrete energy around the level of 10^{-4}.

τ	Leap-Frog		IRK2-MC		IRK2-EC		IRK4-MC		IRK4-EC	
	error	rate	error	rate	error	rate	error	rate	error	rate
$\frac{1}{10}$	NA	NA	7.05	NA	3.45	NA	0.35	NA	0.61	NA
$\frac{1}{20}$	NA	NA	3.60	1.96	0.72	4.80	$1.6e-2$	21.6	$1.3e-2$	46.8
$\frac{1}{40}$	6.88	NA	1.02	3.53	0.18	4.05	$8.9e-4$	18.6	$5.6e-4$	23.2
$\frac{1}{80}$	1.92	3.59	0.26	3.93	0.44	4.03	$6.7e-5$	13.2	$5.1e-5$	10.9

TABLE 2. The convergence rates of Leap-Frog, IRK2-MC, IRK2-EC IRK4-MC and IRK4-EC in Example 1.

We also list the L^∞ error $\mathcal{E}^n$ at $t = T$ with different time step τ for these five time integrators in Table 2. One can see that the Leap-Frog, IRK2-MC and IRK2-EC decrease with the ratio around 4, which are as expected, since they are of the second order schemes. On the other hand, the ratio of the 4th order methods IRK4-MC and IRK4-EC is around 2^4, since they are 4th order methods. When the time step τ is small, the decay rate is slightly below 16 (see the last row in Table 2). This is probably because the temporal error becomes comparable to the spatial discretization error, and consequently, affects the ratio.

Example 2. We next consider the scattering solution for the BO equation with the initial condition $u_0 = -2\operatorname{sech}^2(x)$. Its KdV version has been studied for questions on dispersion limit, see, e.g. [30] and [38]. Here, we expect that a similar solution behavior may happen, since the BO equation only changes the dispersion term u_{xxx} from the KdV equation to $\mathcal{H}u_{xx}$ (less amount of dispersion if viewed on the Fourier frequency side). Note that a negative value for $\int u^3 dx$ may occur, and thus, the C_0 adjustment process in (3.16) will make $v(t)$ stay positive, and will keep the algorithm applicable for all time. The exact solution is not explicitly given, since due to the negative sign in the initial condition and coefficients chosen.

In this example, we still take the $N = 1024$ and $\alpha = 25$ for the spatial discretization. The time step $\tau = \frac{1}{400}$ ($\tau = \frac{1}{800}$ for the Leap-Frog) and the stopping time $T = 2$. We compute the reference solution u_{ref} by both IRK4-MC and IRK4-EC methods independently with an ultimately small time step ($\tau = 1/6400$), denoted as $u_{\text{ref}-\text{MC}}$ and $u_{\text{ref}-\text{EC}}$, respectively. Since we intend to track the convergence rate with respect to time, to minimize the influence from the spatial discretization error, we use the $u_{\text{ref}-\text{MC}}$ to compute the L^∞ error $\|\mathbf{u}^n - u_{\text{ref}}\|_\infty$ when the $\mathbf{u}^n$ is obtained by the mass-conservative schemes (IRK2-MC and IRK4-MC), and use the $u_{\text{ref}-\text{EC}}$ to compute the L^∞ error $\|\mathbf{u}^n - u_{\text{ref}}\|_\infty$ when $\mathbf{u}^n$ is obtained by the energy-conservative schemes (IRK2-EC and IRK4-EC) and the Leap-Frog scheme. The spatial discretization error accumulates as the time evolves, see Figure 5. From Figure 5, the difference increases to the level of 10^{-6} between these two solutions by the time we terminate the simulation.

Figure 3 shows the solution profile obtained from the IRK4-EC method. The left subplot shows the solution profile at different times t. The right plot shows the solution at the terminal time $t = 2$. We can see that the solution radiates to the right with fast oscillations. On the other hand, compared with the similar type of solutions to the KdV case (e.g., in
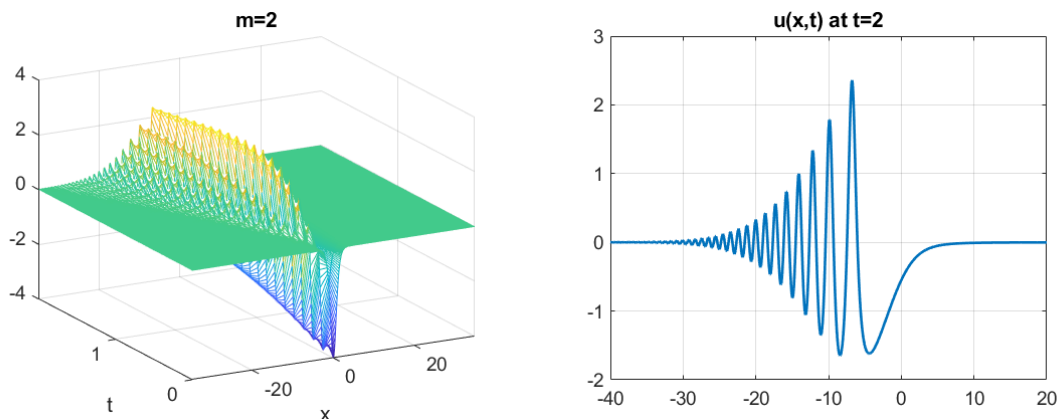
FIGURE 3. The solution profile in Example 2 from IRK4-SAV. Left: $u(x,t)$. Right: $u(x,t)$ at $t = 2$.

	Leap-Frog		IRK2-MC		IRK2-EC		IRK4-MC		IRK4-EC	
τ	error	rate	error	rate	error	rate	error	rate	error	rate
$\frac{1}{200}$	0.104	NA	0.027	NA	0.027	NA	$4.4e-5$	NA	$4.4e-5$	NA
$\frac{1}{400}$	0.026	4.00	$6.7e-3$	3.99	$6.7e-3$	3.99	$2.8e-6$	15.8	$2.8e-6$	15.8
$\frac{1}{800}$	$6.5e-3$	3.99	$1.7e-3$	4.02	$1.7e-3$	4.02	$1.7e-7$	16.0	$1.7e-7$	16.0
$\frac{1}{1600}$	$1.6e-3$	4.00	$4.2e-4$	3.99	$4.2e-4$	3.99	$1.1e-8$	16.0	$1.1e-8$	16.0

TABLE 3. The convergence rates of Leap-Frog, IRK2-MC, IRK2-EC IRK4-MC and IRK4-EC in Example 2.

[37] and [68]), the frequency is smaller. This indicates that the lower order dispersion ($\mathcal{H}\partial_{xx}$ compared with ∂_{xxx}) generates slower oscillations.

Figure 4 tracks the L^∞-error, error of discrete L^1-type integral, mass and energy with respect to time. One can see that the results are similar to the previous example, and also agree with our analysis in Section 2 and 3.

Table 3 shows the L^∞ error at $t = T$ with respect to the different time step τ. The decay rate is on the 2nd order for the 2nd order schemes (Leap-Frog, IRK2-MC and IRK2-EC), and on the 4th order for the 4th order schemes (IRK4-MC and IRK4-EC). Surprisingly, the IRK types of schemes (IRK2-MC and IRK2-EC, IRK4-MC and IRK4-EC) generate almost the same error (up to the decimals that we report) from the different reference solutions ($u_{\mathrm{ref-MC}}$ and $u_{\mathrm{ref-EC}}$). This implies that some possible cancellations may occur between the spatial discretization errors.

Example 3. Our final example considers the mBO ($m = 3$) and the gBO ($m = 4$) cases. We take the initial condition $u_0 = 0.99Q$, where Q is the soliton solution from (4.6) with $c = 1$. In these cases, while there is no explict form for Q, the profile of Q can be obtained numerically, e.g., by the Petviashvili iteration from [53], [55], and its convergence analysis
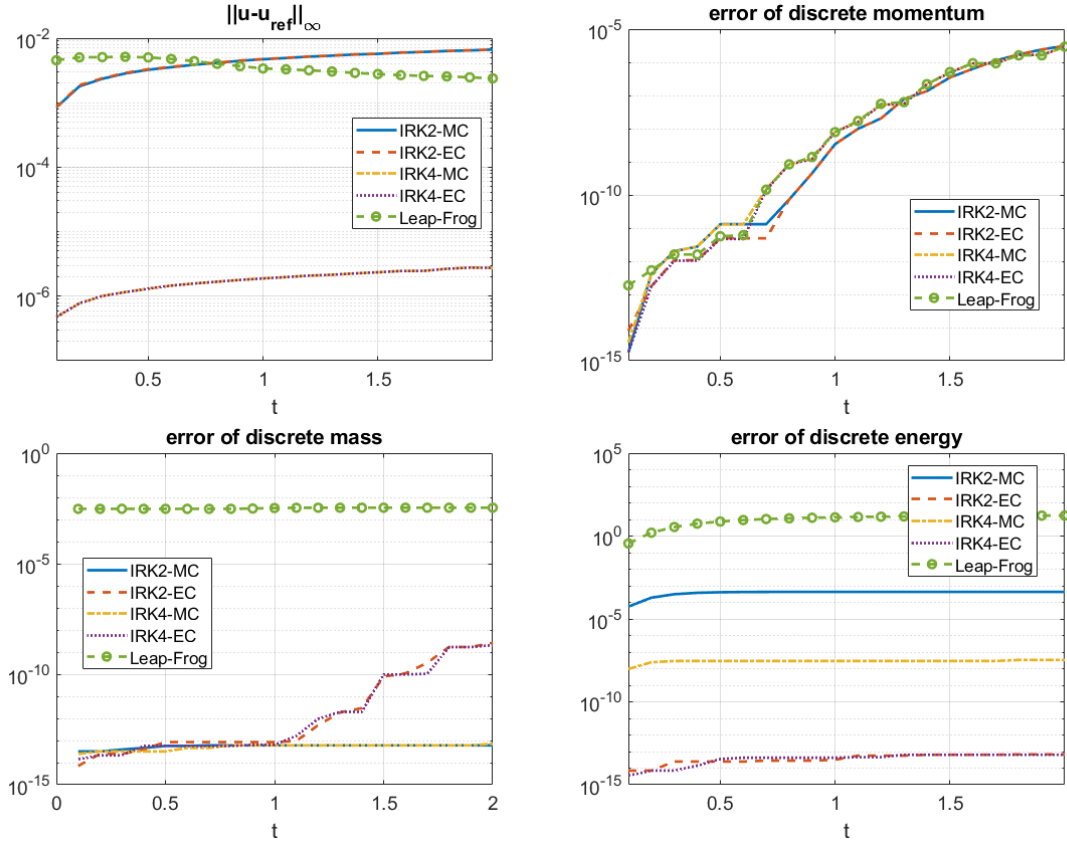
FIGURE 4. The errors in Example 2 by different time integrators: IRK2-MC (solid blue); IRK2-EC(dash red); IRK4-MC (dash dot orange); IRK4-EC (dot purple); Leap-Frog (circle green). Top left: $\|\mathbf{u}^n - u_{\text{ref}}\|_\infty$. Top right: discrete momentum error. Bottom left: discrete mass error. Bottom right: discrete energy error.

in [40], [51] and [42]. From [25], when $u_0 = 0.99Q$, which indicates that the solution is below the mass-energy threshold, the solution is proven to exist globally in time. Recent numerical study in [55] shows that the solution blows up when $u_0 = 1.01Q$. In this paper, we consider the globally existing solutions, and thus, we take $u_0 = 0.99Q$ in our example. We take $N = 1024$, $\alpha = 25$, $\tau = 0.02$ ($\tau = 0.01$ for the Leap-Frog scheme due to the stability issue) in our simulation. We run until $T = 10$ for $m = 3$, and $T = 5$ for $m = 4$.

Figures 6 and 7 show the solution profiles obtained from the scheme IRK4-EC for $m = 3$ and $m = 4$, respectively. The left subplots show the solution profiles $u(x, t)$ at different times. The right subplots show the solution at the final time T (blue solid line) and their comparison with the initial condition u_0 (red dash line). For $m = 3$, the solution travels to the right with some radiation parts scattering to the left. However, for the $m = 4$ case, the solution completely radiates to the left. This agrees with the results in our earlier paper [55].
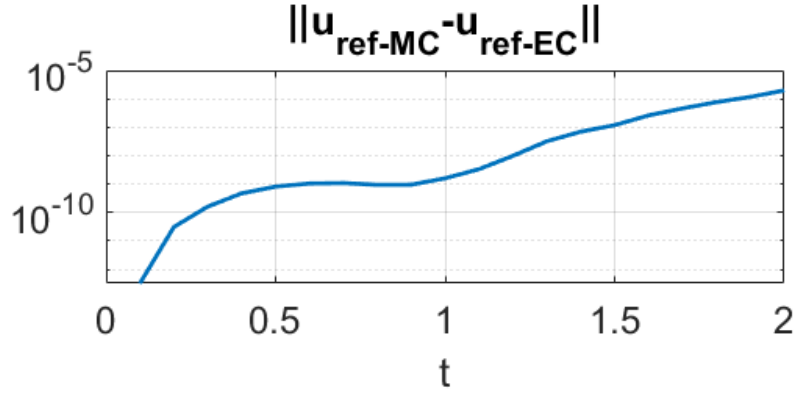
FIGURE 5.   The difference of the reference solution obtained by the IRK4-EC scheme and IRK4-MC scheme. One can see the difference (mainly caused by the spatial discretization) keeps increasing to the level 10^{-6}.
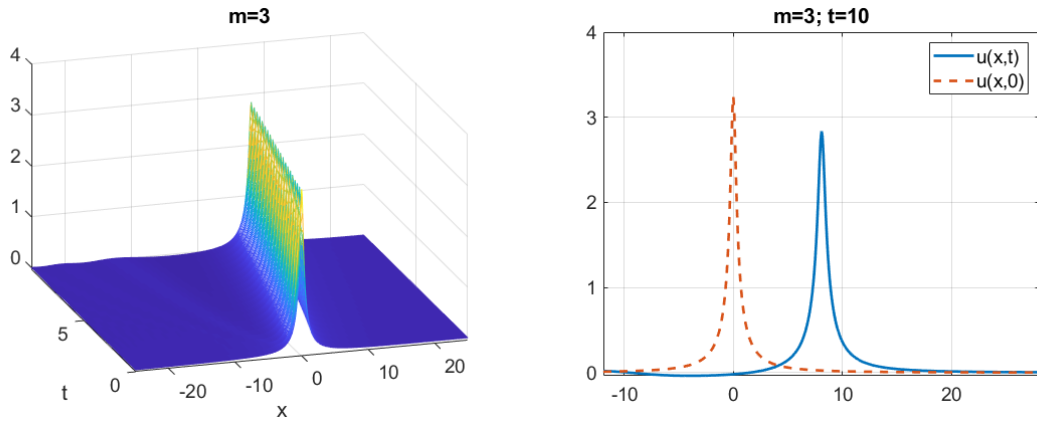

FIGURE 6.   The solution profile in Example 3 from IRK4-EC with $m = 3$. Left: $u(x,t)$. Right: $u(x,t)$ at $t = 10$.

Figure 8 and 9 track the error of discrete L^1-type integral (left subplot), mass (middle subplot) and energy (right subplot) at different times for $m = 3$ and $m = 4$, respectively. Again, the discrete mass or energy can be preserved by choosing the mass-conservative scheme or energy-conservative scheme, respectively, which agrees with the analysis in Sections 2 and 3.

5. CONCLUSION AND OTHER DISCUSSION

We propose two kinds of pseudo-spectral spatial discretization for the generalized Benjamin-Ono equation, one is mass-conservative, and the other one is energy-conservative. Combined with the conservative time discretization, such as the symplectic Runge-Kutta method, arbitrarily high order mass-conservative or energy-conservative numerical schemes can be constructed. In fact, the symplectic Runge-Kutta method with the scalar auxiliary variable
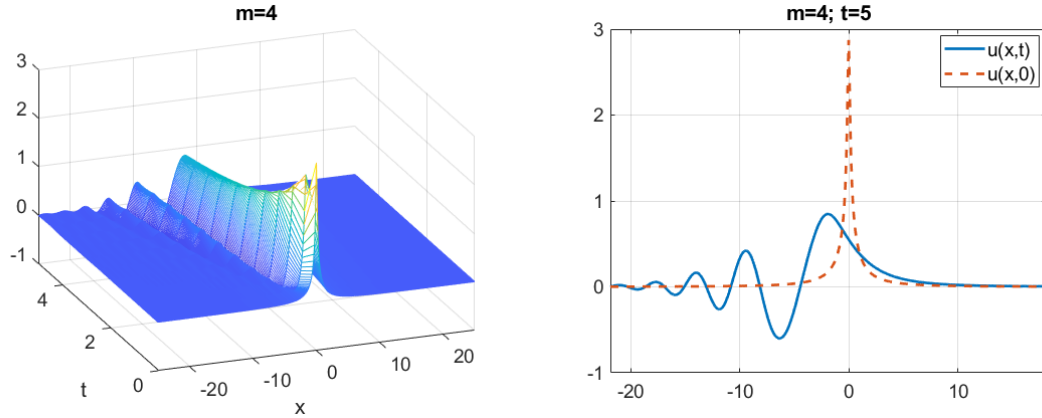
FIGURE 7. The solution profile in Example 3 from IRK4-EC with $m = 4$. Left: $u(x,t)$. Right: $u(x,t)$ at $t = 5$.
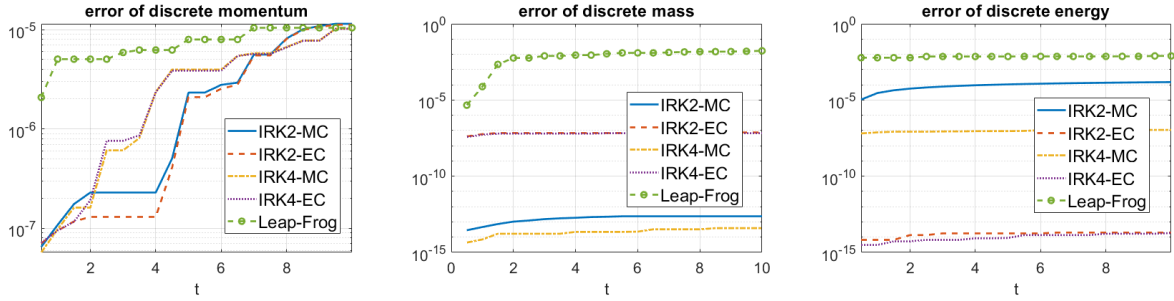

FIGURE 8. The errors in Example 3 ($m = 3$) by different time integrators: IRK2-MC (solid blue); IRK2-EC(dash red); IRK4-MC (dash dot orange); IRK4-EC (dot purple); Leap-Frog (circle green). Left: discrete momentum error. Middle: discrete mass error. Right: discrete energy error.
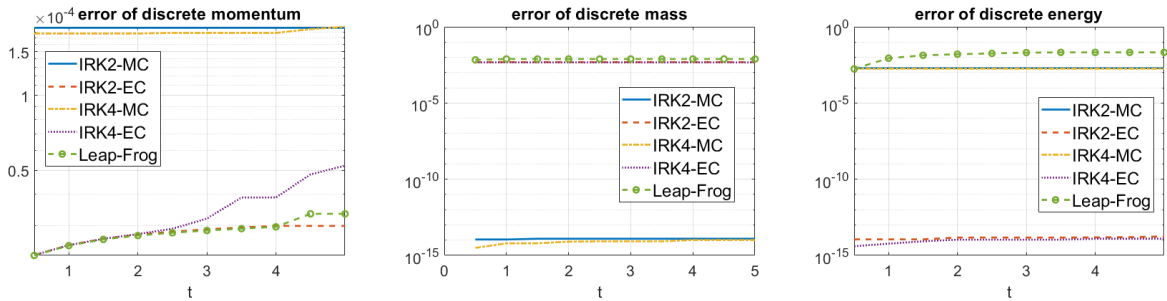

FIGURE 9. The errors in Example 3 ($m = 4$) by different time integrators: IRK2-MC (solid blue); IRK2-EC(dash red); IRK4-MC (dash dot orange); IRK4-EC (dot purple); Leap-Frog (circle green). Left: discrete momentum error. Middle: discrete mass error. Right: discrete energy error.

reformulation preserve all three invariants (1.4)-(1.6) in the discrete time flow. However, the spatial discretization restricts us constructing the scheme to preserve more than one invariant quantity in the fully discrete sense. Numerical results show that the energy-conservative schemes possess superior accuracy compared to the mass-conservative schemes, nevertheless, both of these schemes are more accurate than the non-conservative (Leap-Frog) scheme.

This strategy can be extend to construct the the conservative schemes for the gKdV equations, i.e.,

$$u_t = -u_{xxx} - \frac{1}{m}(u^m)_x;$$

and also the mass-energy conservative (structure-preserving) schemes for the NLS equations, i.e.,

$$u_t = i\left(u_{xx} + |u|^{m-1}u\right).$$

For example, the corresponding spatial semi-discretized form of the equation (3.12) for the gKdV equation will be

$$
\begin{cases}
\mathbf{u}_t = -\mathbf{P^{-1}F^{-1}S_1FP}\left(-\mathbf{P^{-1}F^{-1}S_2FPu} + \frac{1}{m}\frac{\mathbf{u^m}v_h}{\sqrt{\langle\mathbf{u^m,u}\rangle_h + C_0}}\right), \\
(v_h)_t = \frac{m+1}{2\sqrt{\langle\mathbf{u^m,u}\rangle_h + C_0}}\langle\mathbf{u^m, u}_t\rangle_h.
\end{cases}
$$

Similarly, the semi-discretized form for the NLS equation will be

$$
\begin{cases}
\mathbf{u}_t = i\left(-\mathbf{P^{-1}F^{-1}S_2FPu} + \frac{|\mathbf{u}|^{m-1}\mathbf{u}v_h}{\sqrt{\langle|\mathbf{u}|^{m-1}\mathbf{u,u}\rangle_h + C_0}}\right), \\
(v_h)_t = \frac{m}{2\sqrt{\langle|\mathbf{u}|^{m-1}\mathbf{u,u}\rangle_h + C_0}}\operatorname{Re}\left(\langle|\mathbf{u}|^{m-1}\mathbf{u, u}_t\rangle_h\right).
\end{cases}
$$

The straightforward adaption of proof in Theorem 3.4 will show the energy-conservative result for the gKdV equations, and the structure-preserving result for the NLS equations. These results can also be easily extended to higher dimensions (e.g., Zakharov–Kuznetsov equation or the d-dimensional NLS equation) by applying the tensor product in the spatial discretization. We omit the proof and numerical examples here for conciseness.

In summary, by applying the rational basis functions, the above illustrated conservative schemes will increase the computational efficiency significantly, especially, in tracking the solution's long time behavior, or the slow decaying solutions (e.g., $u_0 = \frac{1}{1+x^2}$), since far less number of nodes are needed compared with the traditional domain truncation approaches.

References

[1] L. Abdelouhab, J. Bona, M. Felland, and J.-C. Saut. Nonlocal models for nonlinear, dispersive waves. *Physica D: Nonlinear Phenomena*, 40(3):360–392, 1989.

[2] M. J. Ablowitz, M. Ablowitz, P. Clarkson, and P. A. Clarkson. *Solitons, nonlinear evolution equations and inverse scattering*, volume 149. Cambridge university press, 1991.

[3] M. J. Ablowitz, A. S. Fokas, and R. L. Anderson. The direct linearizing transform and the Benjamin-Ono equation. *Phys. Lett. A*, 93(8):375–378, 1983.

[4] J. Albert, J. L. Bona, and D. Henry. Sufficient conditions for stability of solitary-wave solutions of model equations for long waves. *Physica D*, 24:343–366, 1987.

[5] T. B. Benjamin. Internal waves of permanent form in fluids of great depth. *Journal of Fluid Mechanics*, 29(3):559–592, 1967.

[6] T. B. Benjamin, J. L. Bona, and J. J. Mahony. Model equations for long waves in nonlinear dispersive systems. *Philosophical Transactions of the Royal Society of London. Series A, Mathematical and Physical Sciences*, 272(1220):47–78, 1972.

[7] T. L. Bock and M. D. Kruskal. A two-parameter Miura transformation of the Benjamin-Ono equation. *Phys. Lett. A*, 74(3-4):173–176, 1979.

[8] J. Bona and H. Kalisch. Models for internal waves in deep water. *Discrete & Continuous Dynamical Systems-A*, 6(1):1–20, 2000.

[9] J. Bona and H. Kalisch. Singularity formation in the generalized Benjamin-Ono equation. *Discrete and continuous dynamical systems*, 11:27–46, 2004.

[10] J. L. Bona, P. E. Souganidis, and W. A. Strauss. Stability and instability of solitary waves of Korteweg-de Vries type. *Proceedings of the Royal Society of London. A. Mathematical and Physical Sciences*, 411(1841):395–412, 1987.

[11] J. P. Boyd. Spectral methods using rational basis functions on an infinite interval. *Journal of Computational Physics*, 69(1):112–142, 1987.

[12] J. P. Boyd. The orthogonal rational functions of Higgins and Christov and algebraically mapped Chebyshev polynomials. *Journal of Approximation Theory*, 61(1):98–105, 1990.

[13] J. P. Boyd and Z. Xu. Comparison of three spectral methods for the Benjamin-Ono equation: Fourier pseudospectral, rational Christov functions and Gaussian radial basis functions. *Wave Motion*, 48(8):702–706, 2011.

[14] J. P. Boyd and Z. Xu. Numerical and perturbative computations of solitary waves of the Benjamin-Ono equation with higher order nonlinearity using Christov rational basis functions. *J. Comput. Phys.*, 231(4):1216–1229, 2012.

[15] N. Burq and F. Planchon. Smoothing and dispersive estimates for 1D Schrödinger equations with BV coefficients and applications. *J. Funct. Anal.*, 236(1):265–298, 2006.

[16] N. Burq and F. Planchon. On the well-posedness of the Benjamin-Ono equation. *Math. Ann.*, 340:497—-542, 2008.

[17] J. C. Butcher. Implicit Runge-Kutta processes. *Mathematics of Computation*, 18(85):50–64, 1964.

[18] C. I. Christov. A complete orthonormal system of functions in $L^2(-\infty, \infty)$ space. *SIAM J. Appl. Math.*, 42(6):1337–1344, 1982.

[19] G. Cooper. Stability of Runge-Kutta methods for trajectory problems. *IMA journal of numerical analysis*, 7(1):1–13, 1987.

[20] J. Cui, Y. Wang, and C. Jiang. Arbitrarily high-order structure-preserving schemes for the Gross–Pitaevskii equation with angular momentum rotation. *Computer Physics Communications*, 261:107767, 2021.

[21] R. E. Davis and A. Acrivos. Solitary internal waves in deep water. *Journal of Fluid Mechanics*, 29(3):593–607, 1967.

[22] A. Debussche and L. Di Menza. Numerical simulation of focusing stochastic nonlinear Schrödinger equations. *Physica D: Nonlinear Phenomena*, 162(3):131–154, 2002.

[23] R. Dutta, H. Holden, U. Koley, and N. H. Risebro. Convergence of finite difference schemes for the Benjamin–Ono equation. *Numerische Mathematik*, 134(2):249–274, Oct 2016.

[24] T. Duyckaerts and F. Merle. Dynamics of threshold solutions for energy-critical wave equation. *Int. Math. Res. Pap. IMRP*, pages Art ID rpn002, 67, 2008.

[25] L. G. Farah, F. Linares, and A. Pastor. Global well-posedness for the k-dispersion generalized Benjamin-Ono equation. *Differential Integral Equations*, 27(7/8):601–612, 07 2014.

[26] A. S. Fokas and M. J. Ablowitz. The inverse scattering transform for the Benjamin-Ono equation—a pivot to multidimensional problems. *Stud. Appl. Math.*, 68(1):1–10, 1983.

[27] S. Geng. Construction of high order symplectic Runge-Kutta methods. *Journal of Computational Mathematics*, pages 250–260, 1993.

[28] Y. Gong, Q. Wang, Y. Wang, and J. Cai. A conservative Fourier pseudo-spectral method for the nonlinear Schrödinger equation. *Journal of Computational Physics*, 328:354–370, 2017.

[29] T. Grava and C. Klein. Numerical solution of the small dispersion limit of Korteweg-de Vries and Whitham equations. *Communications on Pure and Applied Mathematics: A Journal Issued by the Courant Institute of Mathematical Sciences*, 60(11):1623–1664, 2007.

[30] T. Grava and C. Klein. A numerical study of the small dispersion limit of the Korteweg-de Vries equation and asymptotic solutions. *Physica D: Nonlinear Phenomena*, 241(23-24):2246–2264, 2012.

[31] R. James and J. Weideman. Pseudospectral methods for the Benjamin-Ono equation. *Advances in Computer Methods for partial differential equations*, 7:371–377, 1992.

[32] D. J. Kaup, T. I. Lakoba, and Y. Matsuno. Complete integrability of the Benjamin-Ono equation by means of action-angle variables. *Phys. Lett. A*, 238(2-3):123–133, 1998.

[33] D. J. Kaup and Y. Matsuno. The inverse scattering transform for the Benjamin-Ono equation. *Stud. Appl. Math.*, 101(1):73–98, 1998.

[34] C. Kenig and K. Koenig. On the local well-posedness of the Benjamin-Ono and modified Benjamin-Ono equations. *Math. Res. Lett.*, 10:879–895, 2003.

[35] C. Kenig and Y. Martel. Asymptotic stability of solitons for the Benjamin-Ono equation. *Revista Matematica Iberoamericana*, 25:909–970, 2009.

[36] C. E. Kenig, G. Ponce, and L. Vega. On the generalized Benjamin-Ono equation. *Trans. Amer. Math. Soc.*, 342:155–172, 1994.

[37] C. Klein and J.-C.Saut. IST versus PDE, a comparative study, in Hamiltonian Partial Differential Equations and Applications. *Fields Institute Communications*, 75:383–449, 2015.

[38] C. Klein and R. Peter. Numerical study of blow-up and dispersive shocks in solutions to generalized Korteweg-de Vries equations. *Phys. D*, 304/305:52–78, 2015.

[39] H. Koch and N. Tzvetkov. On the local well-posedness of the Benjamin-Ono equation on $H^s(\mathbb{R})$. *Int. Math. Res. Not.*, 26:1449–1464, 2003.

[40] T. Lakoba and J. Yang. A generalized Petviashvili iteration method for scalar and vector hamiltonian equations with arbitrary form of nonlinearity. *Journal of Computational Physics*, 226(2):1668–1692, 2007.

[41] O. Landoulsi, S. Roudenko, and K. Yang. Interaction with an obstacle in the 2d focusing nonlinear Schrödinger equation. *arXiv preprint arXiv:2102.02170*, 2021.

[42] U. Le and D. E. Pelinovsky. Convergence of Petviashvili's Method near Periodic Waves in the Fractional Korteweg–de Vries Equation. *SIAM Journal on Mathematical Analysis*, 51(4):2850–2883, 2019.

[43] H. Liu and J. Yan. A local discontinuous Galerkin method for the Korteweg-de Vries equation with boundary effect. *Journal of Computational Physics*, 215(1):197–218, 2006.

[44] H. Liu and N. Yi. A Hamiltonian preserving discontinuous Galerkin method for the generalized Korteweg–de Vries equation. *Journal of Computational Physics*, 321:776–796, 2016.

[45] Z. Liu, H. Zhang, X. Qian, and S. Song. Mass and energy conservative high order diagonally implicit Runge-Kutta schemes for nonlinear Schrödinger equation in one and two dimensions. *arXiv preprint arXiv:1910.13700*, 2019.

[46] A. Millet, A. D. Rodriguez, S. Roudenko, and K. Yang. Behavior of solutions to the 1d focusing stochastic nonlinear Schrödinger equation with spatially correlated noise. *Stochastics and Partial Differential Equations: Analysis and Computations*, pages 1–50, 2021.

[47] T. Miloh, M. Prestin, L. Shtilman, and M. Tulin. A note on the numerical and N-soliton solutions of the Benjamin-Ono evolution equation. *Wave Motion*, 17(1):1–10, 1993.

[48] L. Molinet and F. Ribaud. Well-posedness results for the generalized Benjamin-Ono equation with arbitrary large initial data. *Int. Math. Res. Not.*, 70:3757–3795, 2004.

[49] L. Molinet and F. Ribaud. Well-posedness results for the generalized Benjamin-Ono equation with small initial data. *J. Math. Pures Appl.*, 83:277–311, 2004.

[50] A. Nakamura. A Direct Method of Calculating Periodic Wave Solutions to Nonlinear Evolution Equations. I. Exact Two-Periodic Wave Solution. *Journal of the Physical Society of Japan*, 47(5):1701–1705, 1979.

[51] D. Olson, S. Shukla, G. Simpson, and D. Spirn. Petviashvilli's method for the Dirichlet problem. *J. Sci. Comput.*, 66(1):296–320, 2016.

[52] H. Ono. Algebraic solitary waves in stratified fluids. *Journal of the Physical Society of Japan*, 39(4):1082–1091, 1975.

[53] D. E. Pelinovsky and Y. A. Stepanyants. Convergence of Petviashvili's iteration method for numerical approximation of stationary solutions of nonlinear wave equations. *SIAM J. Numer. Anal.*, 42(3):1110–1127, 2004.

[54] B. Pelloni and V. Dougalis. Numerical solution of some nonlocal, nonlinear dispersive wave equations. *J. Nonlinear Sci.*, 10(1):1–22, 2000.

[55] S. Roudenko, Z. Wang, and K. Yang. Dynamics of solutions in the generalized Benjamin-Ono equation: A numerical study. *Journal of Computational Physics*, 445:110570, 2021.

[56] J. Sanz-Serna. Runge-Kutta schemes for Hamiltonian systems. *BIT Numerical Mathematics*, 28(4):877–883, 1988.

[57] J. Sanz-Serna and L. Abia. Order conditions for canonical Runge-Kutta schemes. *SIAM Journal on Numerical Analysis*, 28(4):1081–1096, 1991.

[58] J. Saut. Benjamin-Ono and Intermediate Long Wave equations: Modeling, IST and PDE. *In: Miller P., Perry P., Saut JC., Sulem C. (eds) Nonlinear Dispersive Partial Differential Equations and Inverse Scattering. Fields Institute Communications*, 83. Springer, New York, NY.:95–160, 2018.

[59] J.-C. Saut. Sur quelques généralisations de l' équation de Korteweg-de Vries. *J. Math. Pures Appl.*, 58:21–61, 1979.

[60] J. Shen, T. Tang, and L.-L. Wang. *Spectral methods*, volume 41 of *Springer Series in Computational Mathematics*. Springer, Heidelberg, 2011. Algorithms, analysis and applications.

[61] J. Shen, J. Xu, and J. Yang. The scalar auxiliary variable (SAV) approach for gradient flows. *Journal of Computational Physics*, 353:407–416, 2018.

[62] J. Shen, J. Xu, and J. Yang. A new class of efficient and robust energy stable schemes for gradient flows. *SIAM Review*, 61(3):474–506, 2019.

[63] T. Tao. Global well-posedness of the Benjamin-Ono in $H^1(\mathbb{R})$. *J. Hyperbolic Diff. Eq.*, 1(1):27–49, 2004.

[64] V. Thomée and A. V. Murthy. A numerical method for the Benjamin-Ono equation. *BIT Numerical Mathematics*, 38(3):597–611, 1998.

[65] L. N. Trefethen. *Spectral methods in MATLAB*, volume 10 of *Software, Environments, and Tools*. Society for Industrial and Applied Mathematics (SIAM), Philadelphia, PA, 2000.

[66] S. Vento. Sharp well-posedness results for the generalized Benjamin-Ono equation with high nonlinearity. *Differ. Integr. Equ.*, 22(5-6):425–446, 2009.

[67] J. A. C. Weideman. Computing the Hilbert transform on the real line. *Math. Comp.*, 64(210):745–762, 1995.

[68] K. Yang. Arbitrarily high-order conservative schemes for the generalized Korteweg-de Vries equation. *arXiv preprint arXiv:2103.13608*, 2021.

[69] N. Yi, Y. Huang, and H. Liu. A direct discontinuous Galerkin method for the generalized Korteweg-de Vries equation: energy conservation and boundary effect. *Journal of Computational Physics*, 242:351–366, 2013.

Florida International University